12.307 Todd Mooring

March 29, 2011

Mass and Wind Lab Report (Draft 2)

Abstract

Vortices are frequently observed in the atmosphere and the oceans. A method is presented for creating a vortex in the laboratory and then its behavior is systematically compared to atmospheric data from a tropical cyclone. The laboratory apparatus, a rotating and draining tank of water, is described and used to study the force balance in the vortex and whether the flow conserves angular momentum. The observations suggest that the flow does conserve angular momentum, and that water parcels retain the angular momentum associated with their initial position in the tank. Surface wind data from the QuikSCAT satellite mission and upper-air analyses are used to study the flow of air in and around Hurricane Katrina. We discuss the wind velocity fields and force balances present in hurricanes and use the Rossby number to relate them to the laboratory experiment. The hurricane upper-air flow is found to be accurately described by gradient wind balance.

Introduction

The atmosphere is a vast body of rotating, stratified fluid. Because it is so large compared to human beings and their devices, it can seldom be experimentally manipulated for scientific study. However, because the qualitative behavior of a fluid dynamical system is frequently controlled by dimensionless numbers formed from the parameters of the system, it is possible to acquire insight about planetary-scale fluid dynamics by conducting laboratory experiments that possess the same dimensionless numbers as the planetary flows, while remaining small enough for easy construction and observation.

This concept can be used to create a laboratory analog of the low-level atmospheric flow into a hurricane. The momentum equation for an inviscid fluid on a rotating planet is

$$\frac{D\vec{u}}{Dt} = -\frac{1}{\rho}\nabla p - f\,\hat{z}\times\vec{u} - \nabla\Phi, \tag{1}$$

where $f = 2\Omega\sin(\phi)$ with Ω the angular rotation velocity of the planet and ϕ the latitude at which the equation is being solved (Marshall and Plumb 2008). Φ is an effective potential that combines both the gravitational and centrifugal forces.

f is known as the Coriolis parameter and is twice the component of the planet's rotation vector in the direction of the frame's local vertical (defined as the direction of $\nabla\Phi$). For $\phi = 0^\circ$ the rotation and local vertical vectors are orthogonal and the projection is zero and for $\phi = 90^\circ$ (rotation and local vertical vectors parallel) the projection is maximized.

Suppose that features in a flow characterized by equation (1) have a characteristic size *L* and vary over characteristic timescale *T*. The flow should thus have a characteristic velocity $U = L/T$. The acceleration term $D\vec{u}/Dt$ has a characteristic scale $U/T = U^2/L$ while the Coriolis term has scale fU. The ratio of the magnitude of the acceleration term to the magnitude of the Coriolis term is referred to as the Rossby number

$$Ro = \frac{1}{|f\,\vec{u}|}\left|\frac{D\vec{u}}{Dt}\right|, \tag{2}$$

which characterizes the relative importance of the acceleration and Coriolis terms in the momentum equation (Marshall and Plumb 2008). It will be shown that the laboratory vortex and real-world hurricanes explore the same regime of *Ro*, and thus have similar dynamical behavior.

Experimental Design and Data Collection

The experimental apparatus is depicted in Fig. 1. It consists of a cylindrical tank of water placed on a rotating table, with a hole in the center of the tank's bottom so the water can drain out. To track the flow, paper dots are floated on the surface of the water in the tank and filmed

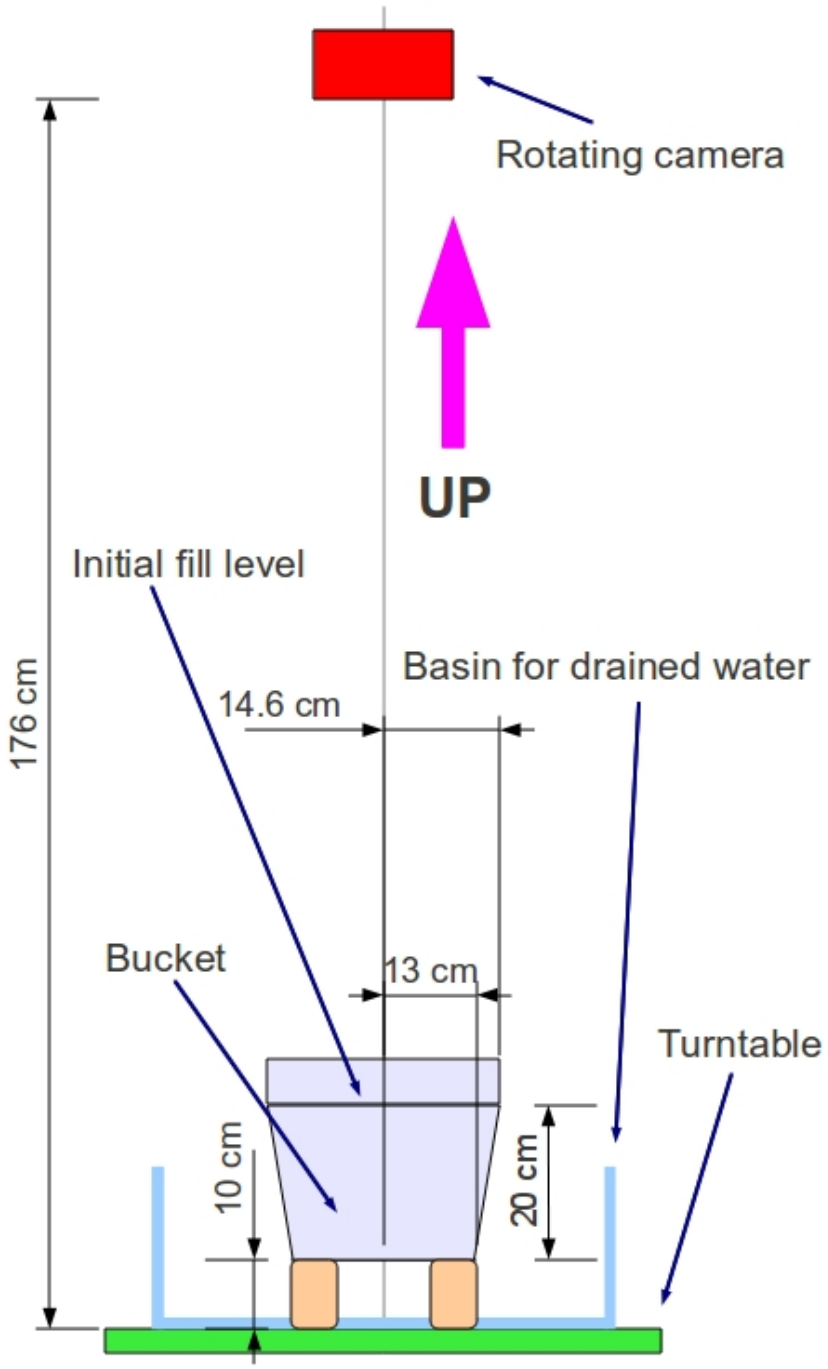

Fig. 1—Diagram of the experimental apparatus The support base and motor for the table and the support bracket for the table, as well as the associated control computers, are not shown. A hole is punched in the center of the bucket to let the water flow out, and the bucket is centered on the rotation axis of the table. During the experiment, water flows out of the hole from the bucket (purplish blue) into a holding basin (turquoise blue). The labeled dimensions are drawn approximately to scale.

using a video camera suspended above the tank. The tank and camera rotate together, which means that the resulting video of the particles essentially depicts their motion in the rotating frame of reference of the table. The experiment begins with the water in solid-body rotation (in other words, at rest in the rotating reference frame of the tank), with the hole blocked by a cork to prevent draining. When the cork is removed, draining starts and a vortex is created.

Equation (1) can be used to describe the draining tank as well, provided the centrifugal force is subsumed into the pressure gradient term instead of the gravitational potential term in a manner to be described later. The most important parameter controlled by the experimenter in equation (1) is f. Because the rotation vector and $\nabla\Phi$ are essentially parallel, $\phi = 90^\circ$ and $f = 2\Omega$. The experiment was carried out four times, each with a different value of f, as summarized in Table 1. Usually multiple tracking particles were placed on the surface during each experiment. However, the video tracking system was not able to successfully follow all the particles used in each experiment. The number of unique and useful tracks available for each value of f is listed in Table 1.

Table 1—Particle tracks obtained from rotating tank vortex experiments

f (rad s^{-1})	Useful tracks	Notes
0.500	3	Used for angular momentum conservation analysis, less tight spirals than f = 1 and f = 2.002 rad s^{-1}
1	2	
2.002	3	Used for angular momentum conservation analysis
4.003	0	

The particle tracking software returned particle positions as a function of time in the pixel

(Cartesian) coordinates of the camera[1]. After the valid and useful segments of particle tracks were identified, the particles' coordinates were transformed into a drain-centered pixel-based Cartesian coordinate system. (The drain location was identified by inspection of plots of the particle tracks.)

During the experiment, the video camera was used to measure the apparent diameter of the bucket's rim in pixels to facilitate conversion of the pixel positions to real length units[2]. Additional measurements with a ruler were used to determine a pixels-to-cm conversion scale for the data. The cm-based Cartesian coordinate system was then converted to a polar coordinate system to facilitate further data analysis.

Analysis—Rossby Number and Angular Momentum Conservation

The particle trajectories for the $f = 0.500$ rad s^{-1} and $f = 1$ rad s^{-1} are plotted in Fig. 2. The generally axisymmetric and rotational nature of the flow is clearly seen, with the particles revolving about the drain hole much more rapidly than they move inwards. Because the direction of fluid flow is primarily in the azimuthal direction with slowly-varying speed, the flow

---

1 For reasons unclear the tracking software sometimes concatenated lists of positions for multiple particles into a single "track", necessitating that each track be plotted and manually checked to remove duplicated tracks. In addition, the increase in angular velocity as particles approached the drain hole could result in track plots that appeared highly jagged because of the decline in the number of positions recorded per revolution of the particle around the drain. Such track sections were deleted from further analysis.

2 Curiously the camera appeared to show the circular bucket rim as somewhat elliptical, with the diameter along the y-axis of the camera coordinate system about 10% longer than along the x-axis. Although later tests suggest that this phenomenon is likely explained by the use of an incorrect setting in the particle tracking software (rather than an actual camera problem of some sort), the spurious ellipticity clearly needed a correction. This was applied by using the bucket diameter measurements to estimate the amount of the ellipticity and then dividing all y-axis position values by 1.103.

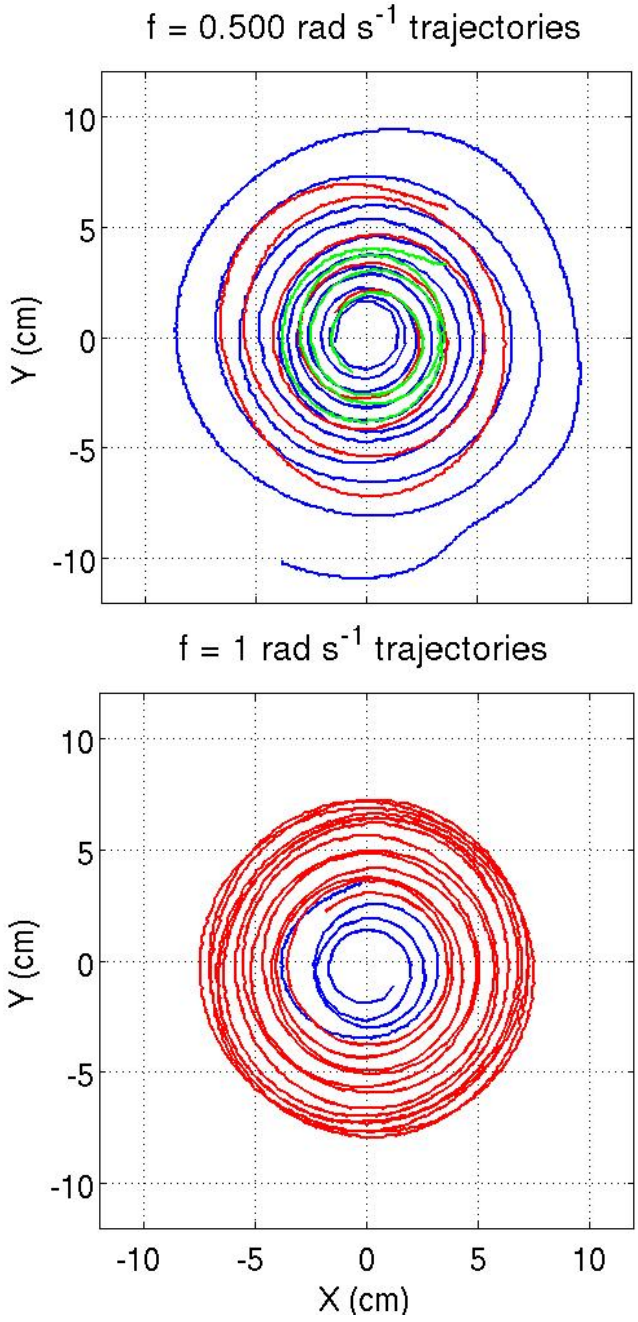

Fig. 2—Particle trajectories The useful parts of the particle trajectories for two of the four experiments are shown here. The particles move counterclockwise and each particle tracked is designated with a different color. The coordinate systems are defined so that the origin is at the drain hole in the center of the tank. Note that the spirals for the $f = 1$ rad s^{-1} experiment appear more tightly wound than those for $f = 0.500$ rad s^{-1}. This makes physical sense: were the tank not rotating ($f = 0$ rad s^{-1}), water would flow approximately straight into the hole and there would be essentially no spiraling. Neither plot has been corrected for the effects of changing water level in the tank.

is near uniform circular motion and thus its acceleration is primarily in the radial direction.

We will develop the relevant theory following (Marshall 2011). For the hurricane flow, the radial component of equation (1) describes the gradient wind balance

$$\frac{v_\theta^2}{r} = \frac{1}{\rho}\frac{\partial p}{\partial r} - f v_\theta = g\frac{\partial h}{\partial r} - f v_\theta, \tag{3}$$

where v_θ is the velocity in the azimuthal direction, measured in the rotating reference frame of the Earth, *g* is the strength of gravity, and *h* is the geopotential height (Illari and Marshall 2009). The second equality is derived using the hydrostatic relationship $\partial p/\partial z = -\rho g$. A similar form of equation (1) can be derived for the rotating tank by beginning in an inertial reference frame with the same origin of the coordinate system as the rotating frame, in which

$$\frac{V_\theta^2}{r} = \frac{1}{\rho}\frac{\partial p}{\partial r} = g\frac{\partial H}{\partial r}, \tag{4}$$

where V_θ is the velocity in the azimuthal direction measured in the inertial frame, *g* is the strength of gravity, and *H* is the height of the surface of the water above the bottom of the tank. Again, the second equality is established by assuming hydrostatic balance (as well as the constancy of ρ). Because $V_\theta = v_\theta + \Omega r$, equation (4) becomes

$$\frac{v_\theta^2}{r} + 2\Omega v_\theta + \Omega^2 r = g\frac{\partial H}{\partial r}, \tag{5}$$

where $\Omega^2 r$ is a centrifugal force term that in equations (1) and (3) has been incorporated into the coordinate system. If we define $h = H - \frac{\Omega^2 r^2}{2g}$, equation (5) can be rewritten as

$$\frac{v_\theta^2}{r} = g\frac{\partial h}{\partial r} - f v_\theta, \tag{6}$$

which is exactly the same functional form as equation (3) for the hurricane.

From equation (2) it is clear that $Ro = v_\theta / fr = \omega / f$, where ω is the angular velocity

of the fluid in the rotating reference frame. It is thus possible to derive an interesting *f*-independent relationship between *Ro* and the radius of a particle from the center of the vortex (Marshall 2011). Again considering the tank experiment in an inertial reference frame, if the flow is approximated as radially symmetric and inviscid water parcels should conserve angular momentum as they flow inward because there is no way for such a flow to generate azimuthal pressure gradients or viscous stresses. Suppose that the water is in solid-body rotation before the cork is pushed out to start draining the tank. Thus a water parcel located at a distance r_1 from the rotation axis will have $V_\theta = \Omega r_1$ with a resulting angular momentum per unit mass of $\Omega r_1^2 = f r_1^2/2$. Because beginning to drain the tank does not change the angular momentum of the fluid parcels, angular momentum conservation implies that, for a given water parcel,

$$L = V_\theta r = (v_\theta + fr/2) r = (\omega + f/2) r^2 = f r_1^2/2 \tag{7}$$

always holds. This relationship should also hold for the hurricane, which we can see by imagining that the region in which the hurricane is located is a flat spinning table with $f = 2\Omega \sin(\phi)$ instead of the $f = 2\Omega$ used in real tank experiments.

Further manipulations of equation (7), including the use of $Ro = \omega / f$, yield

$$Ro = \frac{1}{2}\left(\frac{r_1^2}{r^2} - 1\right), \tag{8}$$

which for appropriate choices of r_1 should hold at least approximately for both tank experiments and the hurricane. It is important to note that because r_1 is the initial radius of a given water parcel it is *not* a constant of the experiment. Water parcels that begin at larger radii have more angular momentum and should retain this angular momentum as they flow inward to the drain. Additionally, equation (8) implies that *Ro* at a given radius for a particular water parcel is a function of r_1.

Equation (7) predicts that $(\omega + f/2)r^2$ is a conserved quantity, and plotting this quantity will help us check the assumption that angular momentum is conserved. In principle it could also shed light on the question of whether r_1 can be identified with the radius of the tank in the tank experiment, as has been suggested.

Before discussing the observed behavior of $(\omega + f/2)r^2$, we will discuss an additional source of systematic error in the measurements of particle position. Referring to Fig. 1, we observe that the water level in the tank can drop by up to 20 cm during an experiment. This causes particles on the surface of the water to move away from the camera, reducing the camera-observed angular distance between the center of the bucket and the particle even if the real radial distance of the particle from the rotation axis of the system remains constant. This concept is further illustrated in Fig. 3.

Suppose that the distance from the camera to the surface of the water at initial time $t = 0$ is D and that after time $t = t_1$ the water level in the bucket has dropped an amount d from its initial level. Making the small angle approximation, a particle a distance r from the rotation axis of the experiment will be observed by the camera to be an angular distance $\theta_i = r/D$ from the rotation axis at the beginning of the experiment and an angular distance $\theta_f = r/(D+d)$ from the axis at time $t = t_1$. Using appropriate values for D and the largest possible value of d, we find that for constant r $\theta_f/\theta_i \approx 0.88$. Because r is squared in $(\omega + f/2)r^2$, this phenomenon could cause angular momentum calculations made for the later part of an experiment to be systematically too small by up to about 20%.

Fig. 4 displays plots of $(\omega + f/2)r^2$ for three particles in the $f = 0.500$ rad s^{-1} experiment. The correction for the changing water depth was applied by assuming that an initial depth of ~20 cm dropped to zero linearly over the full time for which particle tracks were

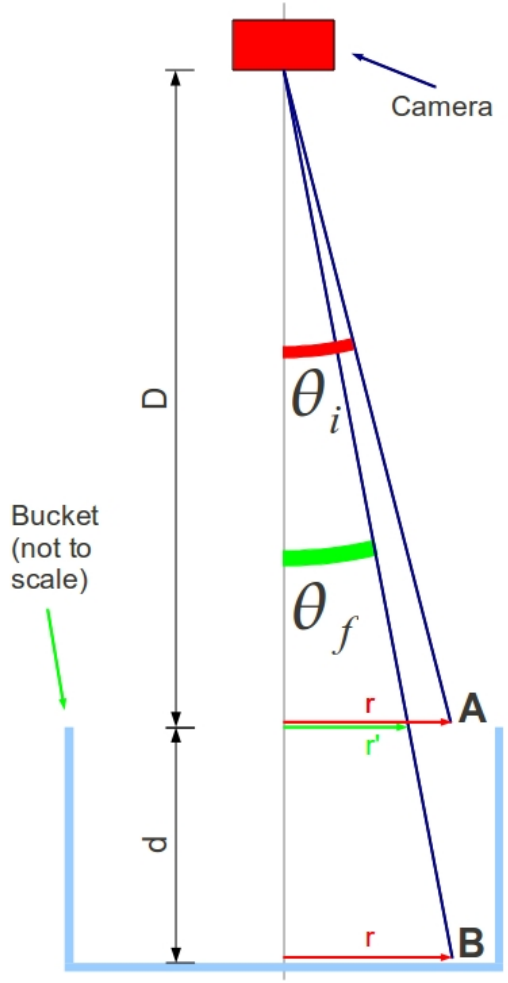

Fig. 3—Geometry of the changing water depth effect Suppose that at the beginning of the experiment a particle is at location A a distance *D* below the camera. We seek to estimate its distance *r* from the rotation axis. Making the small angle approximation, it can be calculated as $r = D\theta_i$ where θ is essentially what is measured by the particle tracker (up to a pixels-to-angle conversion scale). However, if at a later time the water drops a distance *d* below its initial level while remaining at radius *r* (the particle moves to position B), θ declines to θ_f. Multiplying θ_f by *D* will result in an underestimate of the radius $r' = D\theta_f$. To get a correct radius measurement it is necessary to multiply *r′* by (*D*+*d*)/*D*, which yields the correct $r = (D+d)\theta_f$. The data reduction procedure described in the experimental design and data collection section of this report effectively gives *r′*, to which we must apply the correction factor of (*D*+*d*)/*D*.

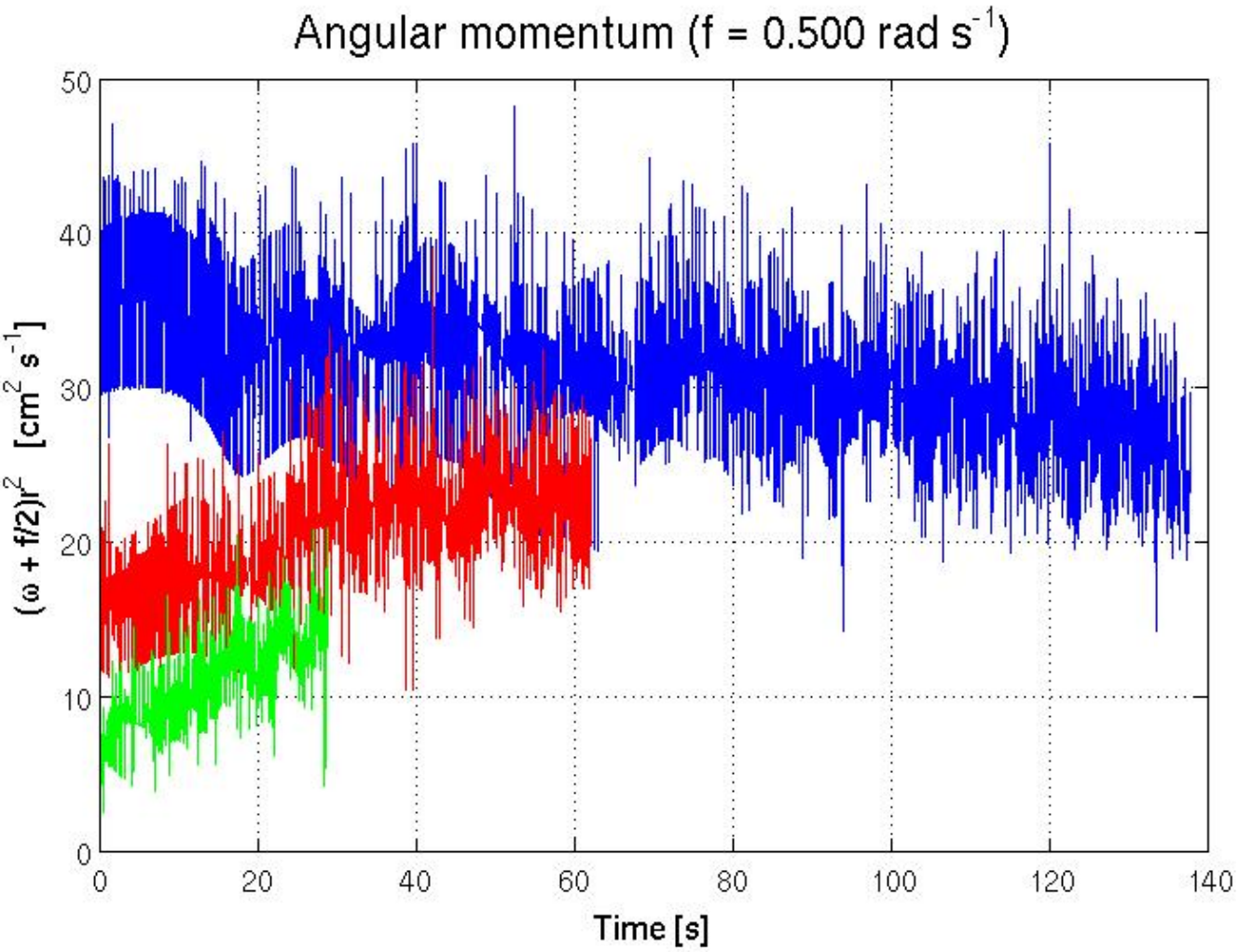

Fig. 4—Particle angular momenta for $f = 0.500$ rad s^{-1} This graph displays the evolution of the angular momentum for the three particles in the $f = 0.500$ rad s^{-1} experiment. No actual measurements were made of the time-dependent water depth during the experiment, so the correction applied for its effect on r and thus the angular momentum must be regarded as a crude approximation. However, calculations suggest that all the results presented in this report are insensitive to the choice of (plausible) assumptions about tank draining behavior.

recorded[3]. Angular momentum conservation is clearly not perfectly satisfied, with two particles actually increasing their angular momenta for unknown reasons. However, the changes in angular momentum experienced by an individual particle over the course of the experiment are generally smaller than the differences in angular momenta between particles. Thus the particles can be reasonably said to have distinct values of angular momentum. This is consistent with the idea that angular momentum is dependent on a particle's initial radius r_1 and inconsistent with the idea that r_1 should be identified with the bucket radius, which is of course the same for all particles.

It is also possible to use angular momentum values computed during the early part of each particle track to directly compute an effective initial radius. Suppose that near the beginning of its track a particle is at radius r_s and is moving with angular velocity ω_s in the rotating reference frame. Assuming equation (7) holds it can be shown that the particle had an initial radius (at which $\omega = 0$) of

$$r_{1\mathrm{eff}} = \sqrt{1 + \frac{2\omega_s}{f}}\, r_s . \tag{9}$$

ω_s and r_s were evaluated by averaging the first 10 available values of ω and r for each track. The values of ω_s, r_s, and r_{1eff} for each particle are given in Table 2.

Table 2—Initial angular velocities and radii and effective initial radii for $f = 0.500$ rad s^{-1}

Particle	ω_s (rad s^{-1})	r_s (cm)	r_{1eff} (cm)
Blue	0.0502	10.9	11.9
Red	0.1251	6.8	8.4
Green	0.0144	4.9	5.0

3 About half of the longest (blue) track was not usable for the angular momentum analysis because the particle was too close to the drain, and this useless half is not plotted in Fig. 3.

Note that because $\omega_s < f/2$ (and usually substantially less than $f/2$) the measured angular momenta are associated primarily with the particles' positions in the tank rather than their angular velocities and thus the particles are fairly close to the initial condition of $L = fr_1^2/2$. Again, the r_{1eff} values are clearly distinct and for two of the three particles are significantly less than the bucket radius of ~14 cm.

Fig. 5 displays the Rossby number as a function of radius for the same three f = 0.500 rad s^{-1} particle tracks shown in Figs. 2 and 3. The crosses denote observed nearly-instantaneous values of *Ro* calculated using ω/f, while the lines are best fits for r_1 to equation (8). For the most part the best-fit lines remain within the scatter of the observed *Ro* values, suggesting that the dependence of *Ro* on *r* is reasonably modeled by equation (8), despite the imperfect assumption of angular momentum conservation[4]. In addition, it is clear that the *Ro* curve for the green particle clearly does not overlap the other two. This can come about only if the curves have distinct values of r_1, which again argues against identification of r_1 with the bucket radius.

Qualitatively similar results on angular momentum conservation and the variation of *Ro* with *r* were obtained using the f = 1 and f = 2.002 rad s^{-1} particle tracks, although the f = 1 rad s^{-1} results are a bit harder to interpret because the water depth effect correction was not applied to relevant plots (not shown). Like the f = 0.500 rad s^{-1} tracks, both tracks for f = 1 rad s^{-1} had their angular momenta initially increase. Apparent periodic variability of the angular momentum was clearly observed on the f = 2.002 rad s^{-1} tracks and one f = 1 rad s^{-1} track[5]. A plot

4 Additionally, an experiment by Malte Jansen showed substantial differences between the motion of particles at the surface of the vortex and the flow of water inside it as indicated by dye. So the particles' angular momentum conservation or lack thereof may not reflect the behavior of the main body of fluid comprising the vortex.

5 For the f = 2.002 rad s^{-1} case at least this may be related to misidentification of the location of the rotation axis. If a particle orbits around the true drain hole, its distance from an incorrect estimated drain hole away from the

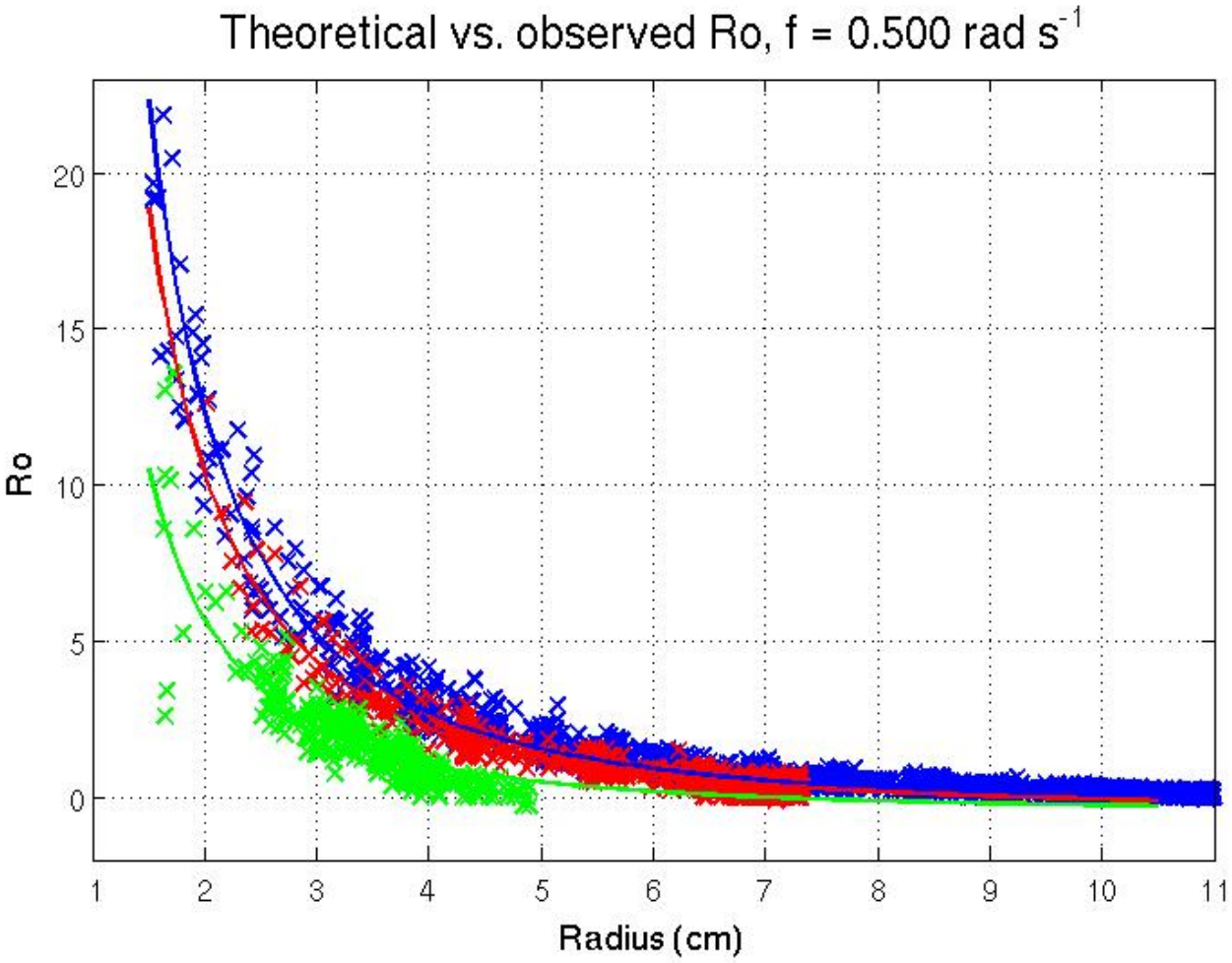

Fig. 5—Variation of *Ro* with radius for $f = 0.500$ rad s^{-1} A plot of the calculated values of the Rossby number as a function of radius for the same three particles whose trajectories were plotted in the upper panel of Fig. 2 and whose angular momenta were plotted in Fig. 4. Fits of the data to equation (8) were performed, and the results are plotted as the solid curved lines. The best-fit values of r_1 for the blue, red, and green tracks are 10.13±0.02, 9.34±0.03, and 7.04±0.06 cm, respectively (Weisstein 2011). Although these regressed values for r_1 do not exactly match the computed values for r_{1eff} printed in Table 2, as they should if the experiment were perfectly described by the axisymmetric angular momentum-conserving theory presented here, for two of the three particles the regressed r_1 and r_{1eff} values differ by only around 15% or less. In addition, the fact that the regressed r_1 values are distinctly different from each other is further evidence that r_1 cannot be identified with the bucket radius.

of *Ro* versus *r* for $f = 2.002$ rad s^{-1} was roughly similar to Fig. 5, although the former plot reached did not reach as large of values of *Ro*.

Hurricane Observations and Analysis

Surface winds over the world's oceans are measured with high spatial resolution by the QuikSCAT satellite using radar observations of waves (JPL WINDS Team, n.d.). These wind observations can be used to study hurricanes at sea, and observations for Hurricane Katrina while it was over the Gulf of Mexico are displayed in Fig. 6. The cyclonic flow pattern, analogous to the tank experiment, is unmistakable.

Some simplifications of equation (3) are helpful in studying the hurricane flow (Marshall 2011). If *Ro*<<1, the acceleration term is negligible and $v_\theta \approx v_g$, where v_g is the geostrophic velocity defined by

$$v_g = \frac{g}{f}\frac{\partial h}{\partial r}. \tag{10}$$

If *Ro*>>1, the Coriolis term is negligible and $v_\theta \approx v_c$ where the cyclostrophic velocity v_c is found from

$$v_c = \sqrt{gr\frac{\partial h}{\partial r}}. \tag{11}$$

Fig. 7 displays *Ro* as a function of radius calculated from the surface wind data displayed in Fig. 6. Although the system radius is more than 6 orders of magnitude larger than the tank experiment, the general shape of the pattern of data in Fig. 7 is similar to that in Fig. 5, the analogous plot for the laboratory experiment. Both have *Ro*<<1 at large radii and *Ro*>>1 at small radii. The maximum values of *Ro* reached are of the same order of magnitude. As stated

---

rotation axis should oscillate with the particle's rotation period. One piece of evidence for this idea is a plot (not shown) of the trajectories of the $f = 2.002$ rad s^{-1} particles, which seems to show them revolving about a point slightly displaced from the estimated rotation axis. This center of revolution may well be the true drain hole.

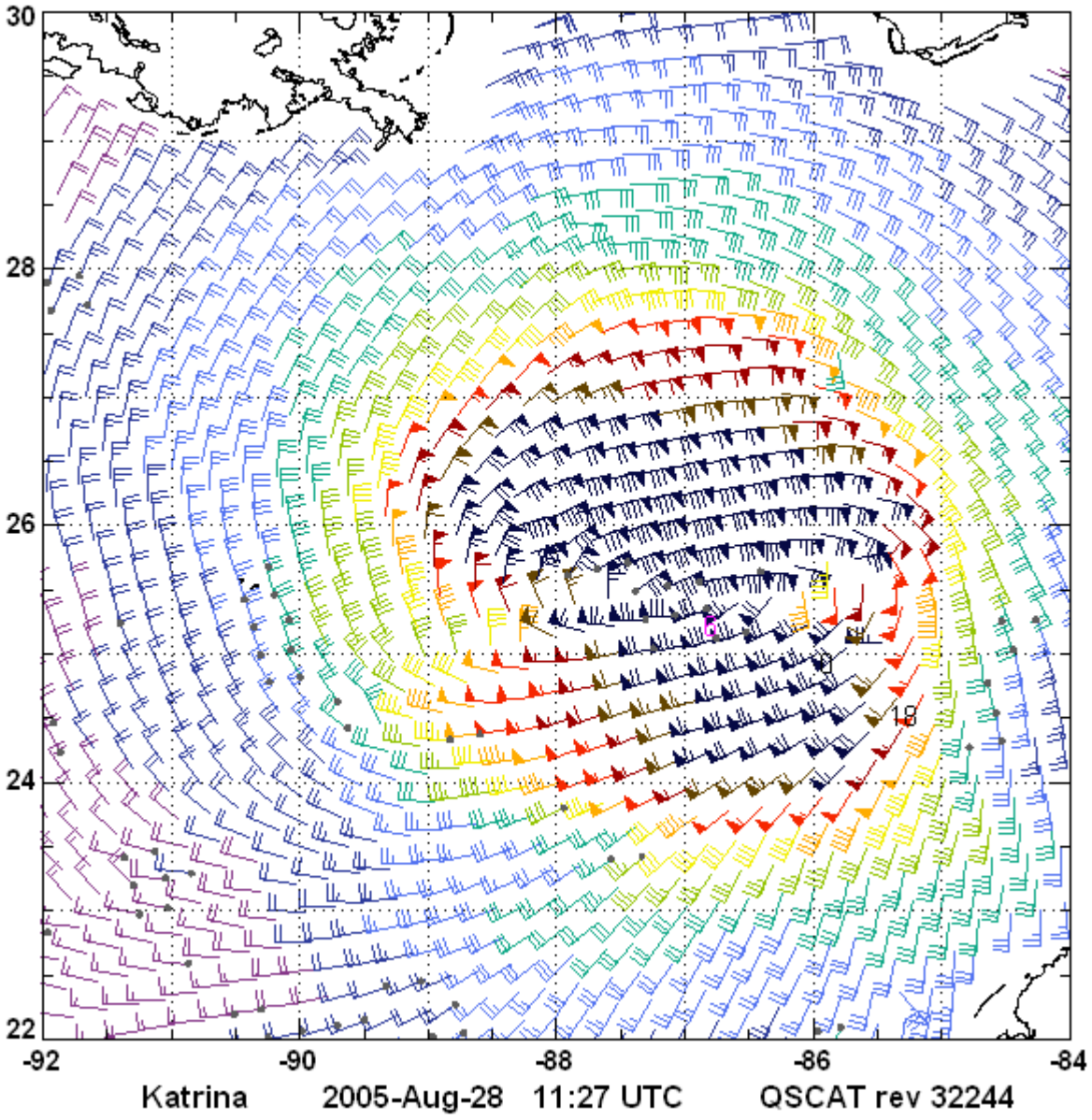

Fig. 6—QuikSCAT surface winds for Hurricane Katrina The wind barbs display the wind speed in knots (Remote Sensing Systems, n.d.). The Louisiana coastline is visible in the northwest corner of the image. If rain could have corrupted the measurements at a particular location, the point of its wind barb is marked with a gray dot. Fortunately there is relatively little such rain corruption.

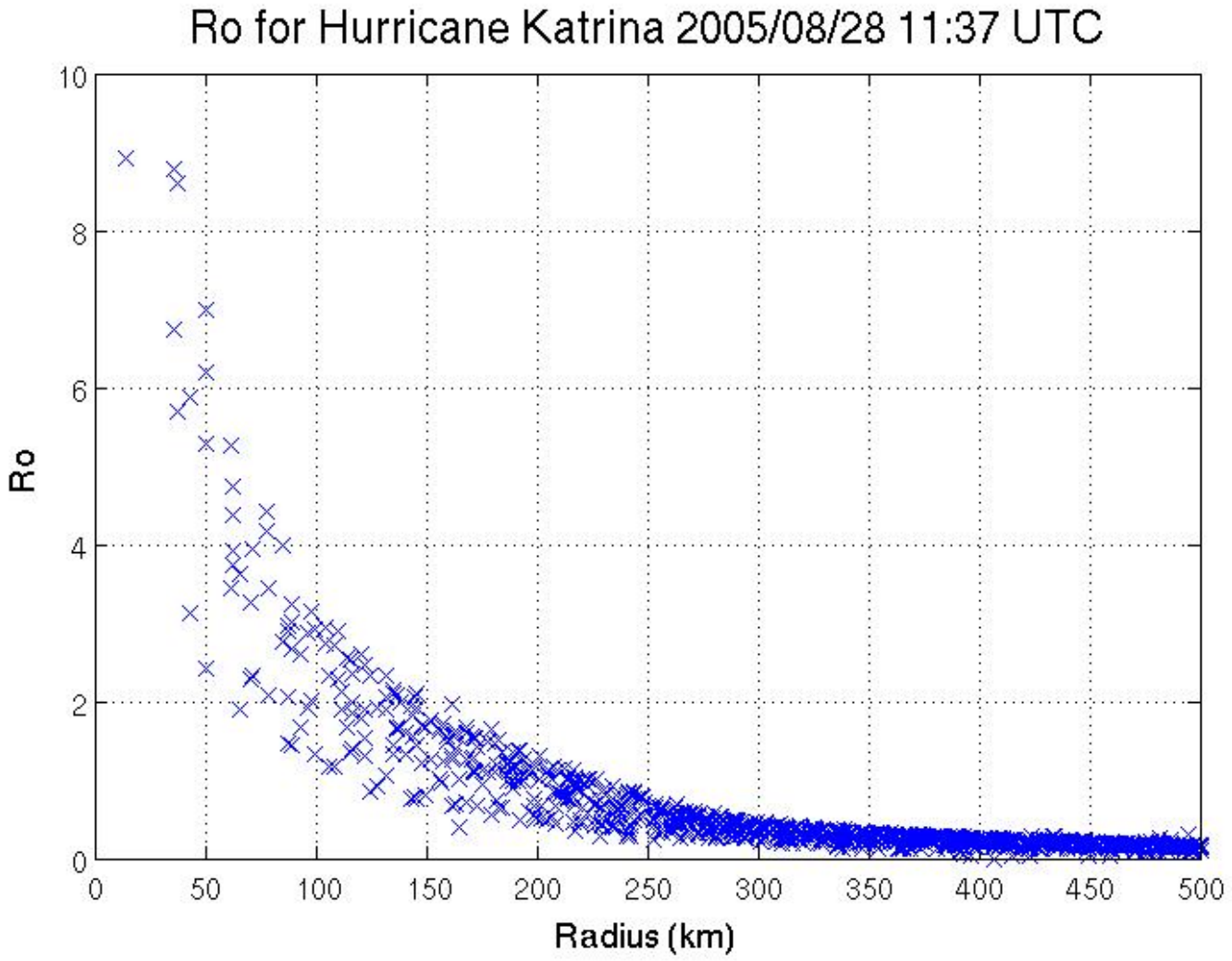

Fig. 7—Rossby number as a function of radius for Hurricane Katrina Values of *Ro* were calculated using the data shown in Fig. 6. Note the striking similarity to Fig. 5, drawn for a much smaller system. The storm center was prescribed as 25.43° N, 87° W. The winds plotted in Fig. 6 were decomposed into azimuthal and radial components in a coordinate system centered at this location, and *Ro* was computed using the azimuthal component only. (In contrast, the calculations presented in Tables 3 and 4 simply assume that the full magnitude of the analyzed wind is in the azimuthal direction.)

previously, this means that the hurricane and the draining tank experiment are in analogous fluid dynamical regimes. Referring to equations (10) and (11), it can be seen that both the tank and the hurricane surface flows are near geostrophic balance at large radii and approach cyclostrophic balance at small radii.

Because QuikSCAT's measuring technique does not work off of the surface, archived operational analyses must be used to study the winds at higher levels. Fig. 8 shows the analyzed 700 mb wind for Hurricane Katrina. As the Rossby number is relatively small for many atmospheric flows, the geostrophic velocity is often useful in analyzing atmospheric motions and Fig. 9 shows the analyzed geostrophic wind for the same time as Fig. 8. For comparison to the 700 mb data, Fig. 10 displays both the observed and geostrophic analyzed winds at 500 mb. Again, cyclonic flow around the storm center is evident. The geostrophic winds are also visibly larger than those actually observed.

However, substantial regions of both the hurricane and the tank are characterized by $Ro \approx 1$. Neither the Coriolis nor the acceleration term can be dropped from the momentum equation. Combining equations (2), (3), and (10), it can be shown that

$$v_g / v_\theta = 1 + Ro. \tag{12}$$

In other words, v_g is always larger than v_θ by an amount that is an increasing function of *Ro*, consistent with Figs. 8-10 (Weather in a Tank Project Team, n.d.). Additionally, the quadratic formula can be used to solve equation (3) for v_θ, producing

$$v_\theta = -\frac{1}{2} fr + \sqrt{\frac{1}{4} f^2 r^2 + gr \frac{\partial h}{\partial r}}. \tag{13}$$

The upper-air analyses can also be used to see if real hurricane flows are quantitatively consistent with the highly simplified theory used to derive equations (12) and (13). Plotting analyzed values of *Ro* calculated using equation (2) at 700 mb, we find that the three circled

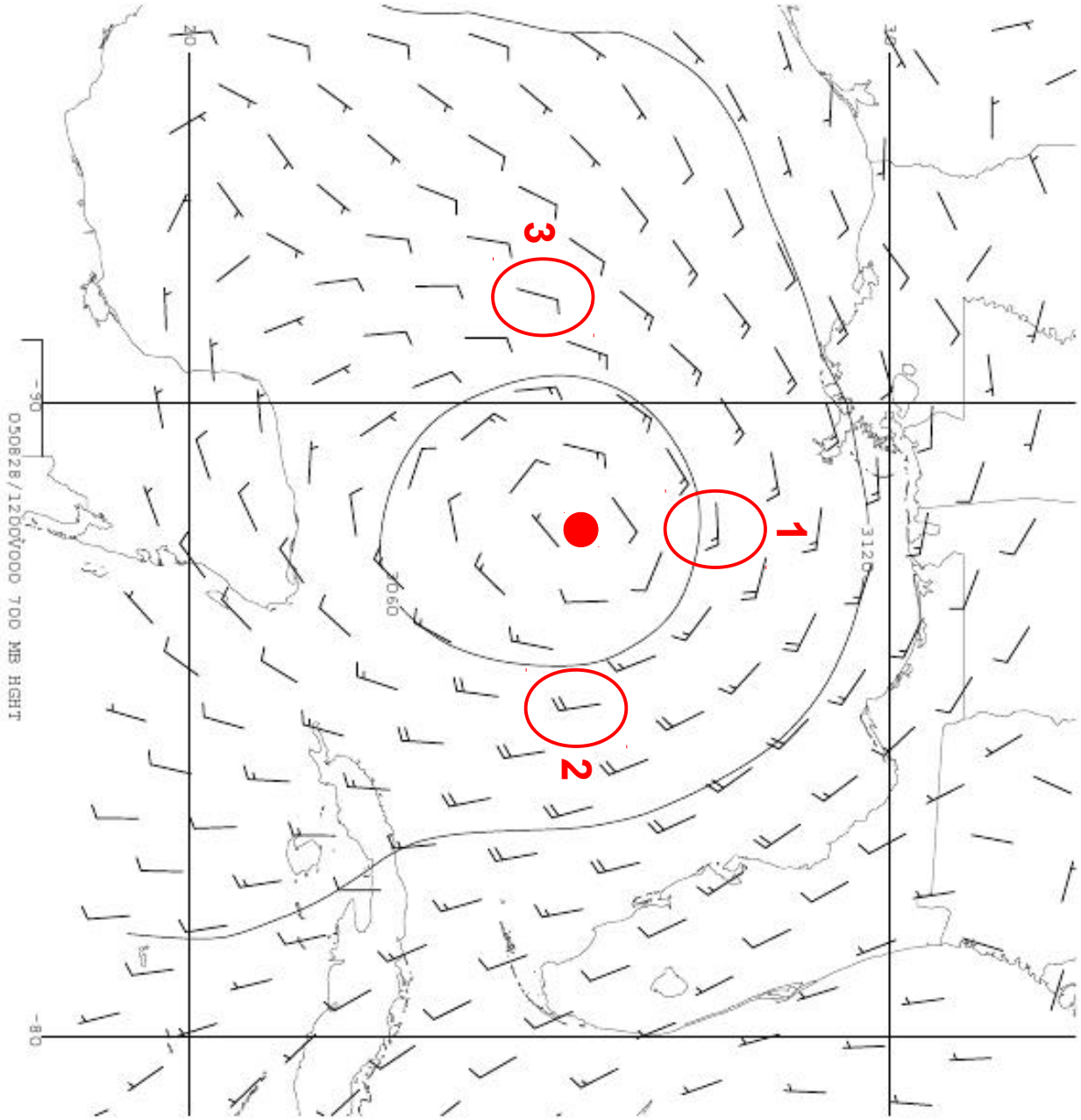

Fig. 8—Observed 700 mb winds for 12Z on 28 August 2005 This is about half an hour after the time for which Fig. 6 is valid. The plotted wind barbs indicate the wind speed in meters per second. The storm center is marked by the red dot, while the locations mentioned in the main text are numbered and circled.

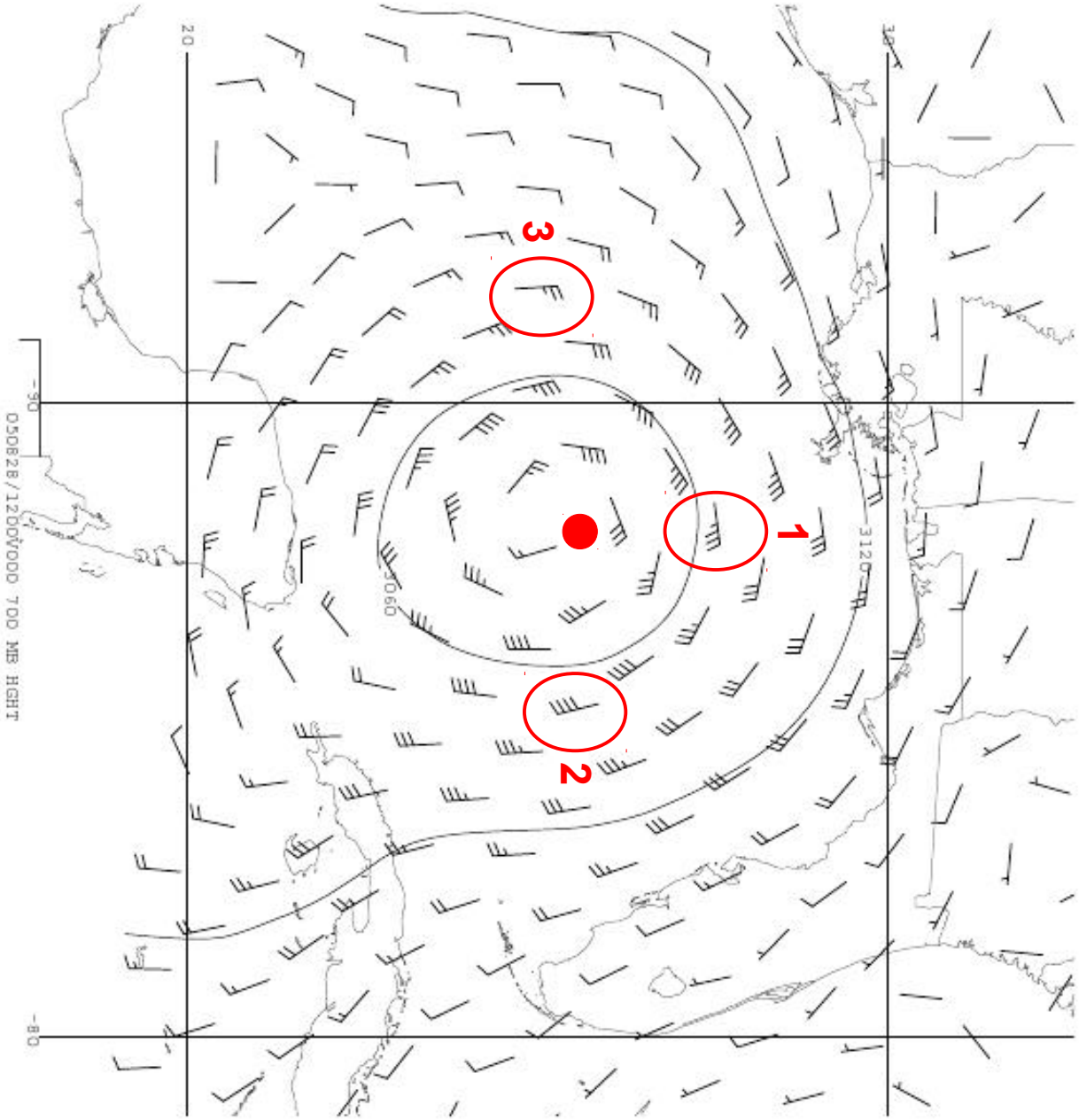

Fig. 9—Geostrophic 700 mb winds at the same time as Fig. 8 The plotted wind barbs indicate the geostrophic wind in meters per second. The geostrophic winds are significantly larger than those observed, as expected. Labeling of the image is the same as for Fig. 8.

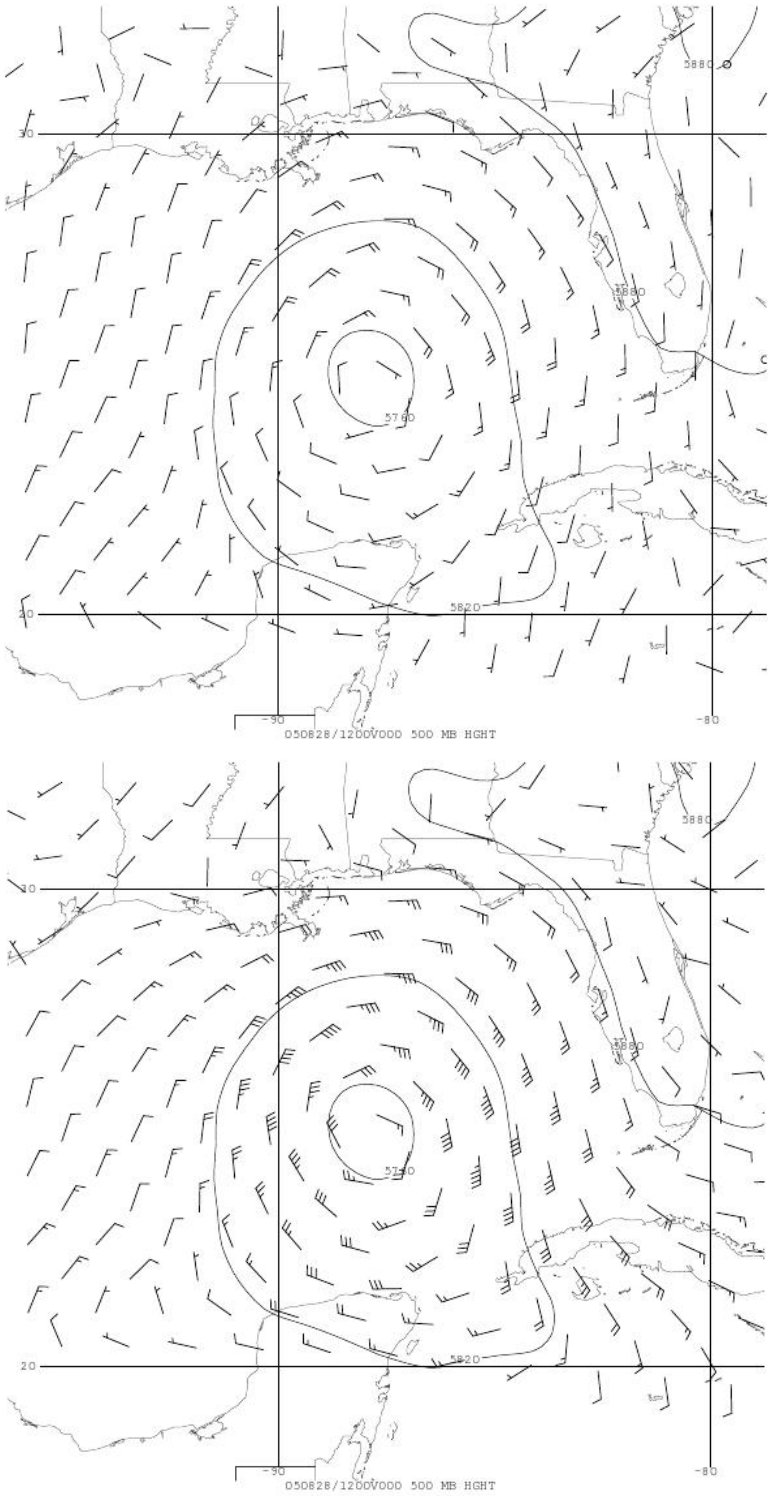

Fig. 10—Analyzed winds at 500 mb for the same time as Figs. 8 and 9 The top panel is the actual winds, the bottom panel is geostrophic winds.

locations in Figs. 8 and 9 have $Ro \approx 1$ (or at least not much less than 1), so that equation (13) must be used to analyze the motions there. We also use the values of v_g and v_θ at the three locations to estimate local values of *Ro* from equation (12). The results are presented in Table 3, and suggest that equation (12) produces substantial overestimates of *Ro*, for reasons that are unclear. However, one obvious possibility is that the imperfect axial symmetry of the storm leads to regions where moving air parcels do not turn much and thus accelerate less than

Table 3—Observed and geostrophic velocities and values of *Ro* in Hurricane Katrina

Location	v_θ **(m s^{-1})**	v_g **(m s^{-1})**	***Ro* from equation (2)**	***Ro* from v_θ and v_g**
1	15	35	0.95	1.33
2	20	40	0.5	1
3	10	25	0.5	1.5

assumed in equation (3).

We will now evaluate the level of agreement between the observations and equation (13) at 700 mb. By measuring Figs. 8 and 9, we are able to obtain approximate values of v_θ, *r*, and $\partial h/\partial r$ appropriate to the three locations circled. We identify *r* as the distance between the circled location and the storm center, and compute $\partial h/\partial r$ by measuring the approximate separation between the geopotential height contours at the locations in question. *f* is evaluated at 25.75° N. Table 4 gives *r*, $\partial h/\partial r$, a theoretical value of v_θ computed using equation (13), and the actual analyzed value of v_θ for each of the three locations circled in Figs. 8 and 9.

Although a full analysis to estimate the uncertainty in the theoretical predictions of v_θ is beyond the scope of this report, the degree of quantitative agreement between the values of v_θ predicted from equation (13) and those actually seen in the atmosphere strongly suggests

that the hurricane flow is well modeled by equation (13). This finding is not too surprising, considering that the hurricane is approximately axisymmetric and has $Ro \approx 1$, two major assumptions of equation (13).

Table 4—Comparison of theoretical and observed values of v_θ for Hurricane Katrina

Location	*r* (km)	$\partial h/\partial r$ (dimensionless)	Theoretical v_θ (m s^{-1})	Analyzed v_θ (m s^{-1})
1	219	2.22×10^{-4}	16	15
2	272	2.35×10^{-4}	18	20
3	407	1.01×10^{-4}	11	10

Conclusion

We have studied the draining of a spinning tank of water and the low-level flow into a hurricane and found them to be similar in key ways. This is because such flows are characterized by their values of the Rossby number $Ro = (1/|f\vec{u}|)|D\vec{u}/Dt|$ and both the draining tank and the hurricane have similar ranges of *Ro*, as seen in Figs. 5 and 7. A partial list of corresponding aspects of the draining tank and hurricane systems is given in Table 5.

Table 5—Analogies between the rotating tank experiment and hurricanes

Rotating Draining Tank	Hurricanes
Spinning table in laboratory	Rotating Earth
Water flows inwards to drain out hole in bottom of tank	Air flows inwards to rise near center of storm
$h = H - \Omega^2 r^2/2g$	Geopotential height

For the tank experiment we attempted to determine if the flow conserves angular momentum. Although angular momentum conservation is not perfect and the data still contain

poorly understood systematic errors, it holds at least approximately for some purposes. An equation for *Ro* as a function of radius in the flow that was derived assuming angular momentum conservation provides a reasonable fit to values of *Ro* computed from observations.

Finally, we evaluated the extent to which upper-air flow in the hurricane was described by gradient wind balance. As expected, geostrophic winds exceeded observed winds although equation (12) does not seem to be quantitatively correct. Good agreement is seen between the values of v_θ predicted from geopotential heights and those actually observed, although this result would be strengthened by a more precise way of carrying out the relevant calculations.

Acknowledgments

Thanks to Reena Joubert for work on the script used to compute the hurricane Rossby number and for generally being such a good lab partner. Malte Jansen performed the experiment suggesting that the paper particles may not in fact be good tracers of water flow in the tank. Tim Cronin's work with the camera system identified the likely cause of the shape distortion problem. Last but certainly not least many thanks are due to Prof. John Marshall and Lodovica Illari for stimulating discussions of the experiment and its results.

References

Illari, L., Marshall, J., 2009. Mass and wind – geostrophic/ageostrophic flow experiment project instructions. Department of Earth, Atmospheric, and Planetary Sciences, Massachusetts Institute of Technology, 5 pp.

JPL WINDS Team, n.d. Missions – SeaWinds on QuikSCAT. Available at http://winds.jpl.nasa.gov/missions/quikscat/index.cfm , accessed 8 March 2011.

Marshall, J., Plumb, R. A., 2008. Atmosphere, ocean, and climate dynamics: an introductory text. Elsevier (Boston), 319 pp.

Marshall, J., 2011. Radial inflow experiment instruction guide. Department of Earth, Atmospheric, and Planetary Sciences, Massachusetts Institute of Technology, 7 pp.

Remote Sensing Systems, n.d. RSS/Tropical Cyclone Microwave Data Archive. Available at http://www.remss.com/cyclone/cyclone.html?year=2005&storm=katrina , accessed 9 March 2011.

Weather in a Tank Project Team, n.d. Balanced Vortex: Theory. Available at http://paoc.mit.edu/labguide/balmo_theory.html , accessed 9 March 2011.

Weisstein, E., 2011. Confidence interval. In: Wolfram MathWorld, Wolfram Research Inc. Available at http://mathworld.wolfram.com/ConfidenceInterval.html, accessed 9 March 2011.